An assessment of the suitability of a Liebau pump in biomedical applications

Joaquín Anatol,[1] Manuel García-Díaz,[2] César Barrios-Collado,[1] José A. Moneo-Fernández,[1] Manuel Rubio,[1] Francisco Castro-Ruiz,[1] and José Sierra-Pallares[1,a)]

[1]Departamento de Ingeniería Energética y Fluidomecánica & ITAP, Universidad de Valladolid, Paseo del Cauce 59, 47011 Valladolid, Spain

[2]Departamento de Energía. Universidad de Oviedo, C/ Wifredo Ricart s/n - Edificio Departamental Este - Campus Universitario, 33204 Gijón, Spain

a) **Author to whom correspondence should be addressed: jsierra@uva.es**

ABSTRACT

Impedance pumping and asymmetric pumping are the main mechanisms of the Liebau effect, a type of valveless pumping. The primary objective of this study is to enhance the current understanding of the mechanics and functionality of a Liebau pump. To achieve this, a prototype pump is constructed, incorporating several novel features: a pinch frequency control system to optimize pump performance, a planar actuator developed using soft robotic technology, and a compliant chamber designed to mitigate flow fluctuations and prevent reverse flow, a common feature of this pumping method. Experimental tests conducted with this prototype demonstrate that the Liebau pump holds potential as a viable technology for fluid pumping in biomedical applications, especially when pulsatile flow is essential or when hemolysis needs to be minimized.

I- INTRODUCTION

The discovery in 1954 of the Liebau phenomenon, which makes it possible to pump fluids without the use of valves, provided an effective alternative to pumping by peristalsis.[1] The Liebau pump is based on the periodic pinching of a compliant tube placed between two rigid tubes, which causes an instantaneous oscillating flow rate. If there is any asymmetry, either in the circuit or in the pinch location or both, a net flow rate, typically pulsing, is produced.[2] The Liebau pump combines two pumping mechanisms: impedance pumping and asymmetric pumping.[3,4]

Anatol et al.[5] described these two pumping mechanisms. Impedance pumping occurs when the pincher is not in the plane of symmetry of the compliant tube [Fig. 1(b)] and the pressure waves are reflected with an offset in the zones of impedance change between the flexible and rigid tubes. This effect creates a pressure gradient that produces

pumping. If the pincher is in the plane of symmetry of the compliant tube, the pressure waves reflected at its ends cancel each other out [Fig. 1(a)]. However, if there is an asymmetry in the hydraulic circuit (in the length, diameter, or material of the rigid tubes), as seen in Fig. 1(c), asymmetric pumping is generated due to the phase shifts of the pressure waves traveling through the circuit. Figure 1(d), in which both effects are superimposed, would correspond to a Liebau pump.

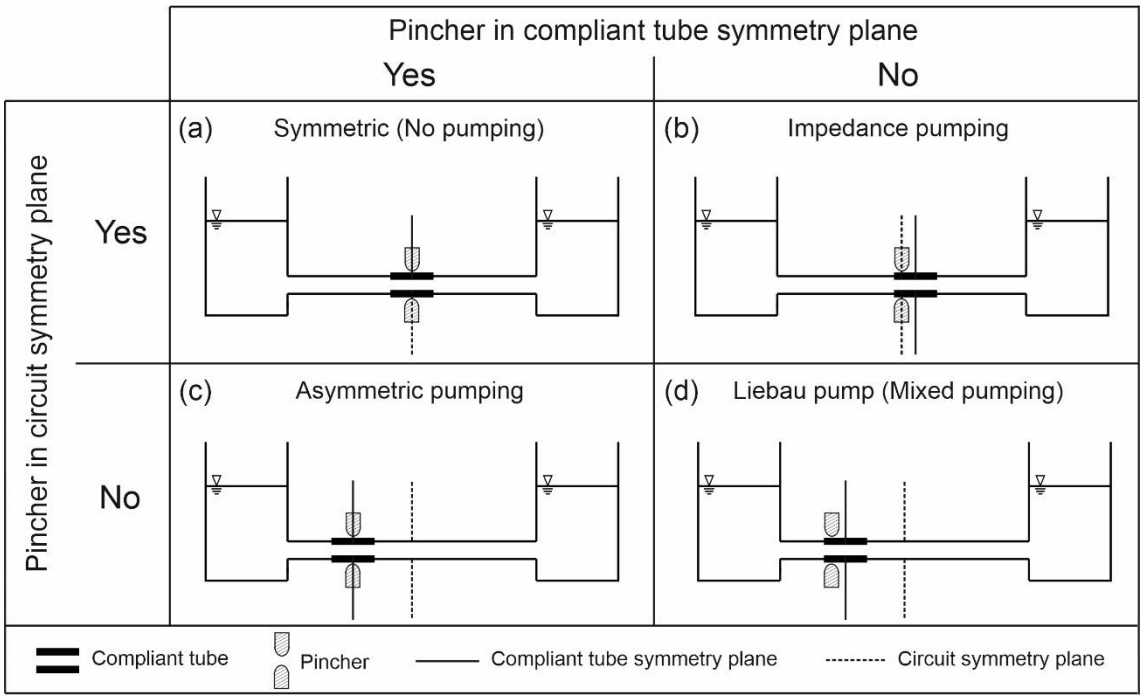

FIG. 1. The pumping mechanisms considered. (a) A symmetric configuration, (b) impedance pumping, (c) asymmetric pumping, and (d) a Liebau pump.

Impedance pumping has been studied extensively through analytical theories,[6–8] mathematical models,[9–15] and experiments.[16–20] One-dimensional models have been developed, such as those proposed by Refs. 13 and 12, and there are more complex models that solve the Navier–Stokes equations, such as those of Refs. 11 and 21. Asymmetric pumping has been studied less than impedance pumping. Among the most prominent researchers are Tagaki and Saijo,[22,23] who experimentally studied this type of pumping. Their results were verified theoretically with a mathematical model based on the mechanical energy conservation equation. The theoretical background of asymmetric pumping was described by Propst[24] using a period-averaged mechanical energy equation. In that research, a system similar to the one shown in Fig. 1(c) was analyzed theoretically. It was shown that the pumping is caused by the difference in kinetic energy between the two rigid pipes, as was also pointed out by Avrahami and Gharib.[11] Propst[24] also found that the difference in the phase average levels of the reservoirs is proportional to the difference in kinetic energy between the two rigid pipes.

In Ref. 4, three open-circuit valveless pumps were characterized — an impedance pump, an asymmetric pump, and a Liebau pump. The effects of the pinching frequency, location, and amplitude on the pump performance were studied. Anatol et al.[5,25] studied asymmetric pumping in an open-circuit installation with a mechanical pincher and another based on soft robotic technology. In their work, the influence on the asymmetric pumping efficiency of the pinch frequency, the duty cycle, the characteristics of the compliant tube, and the geometrical configuration of the circuit were experimentally analyzed.

Unlike peristaltic pumps, the magnitude and direction of a flow generated by a Liebau pump depend nonlinearly on the pinching frequency and duty cycle,[5,6,12,19,25] The performance obtained with Liebau pumps is comparable to that of peristaltic pumps, but with the advantage that a Liebau pump only compresses a small part of the compliant tube.[1,26] The performance of a Liebau pump is very sensitive to the pinching frequency.[19] It is therefore necessary to better understand its behavior in view of possible applications, particularly in the biomedical field.[27] In addition, it will be necessary to develop an industrially applicable design. The resonant pinch frequency (f_R) is the frequency at which the pump performance is best. In applications where the hydraulic configuration of the circuit does not vary, a suitable option to determine the resonant pinch frequency is to perform a frequency sweep.[28] However, in other applications, such as biomedical applications, the circuit hydraulic configuration is variable. Therefore, it is necessary to develop a pinching frequency control system that can detect the resonant value in real time for each cycle.

In this type of pump, the instantaneous flow rate fluctuates significantly and sometimes reverses. Therefore, it is necessary to reduce the fluctuations and the probability of reverse flow for practical use in biomedical applications. In this work, a new frequency control system based on capacitance variation is demonstrated. This approach is shown to be more accurate than one based on instantaneous flow rate variation, which has been used to date.[5,25] A new soft robotic pincher design is also described, which will facilitate the future use of this pump in biomedical applications and also allows the study of the deformation process of the compliant tube. The performances of the two pumping mechanisms in the Liebau pump are compared separately and jointly. Finally, the use of compliant chambers to avoid reverse flow and minimize instantaneous flow fluctuations is analyzed.

II- MATERIALS AND METHODS

A- Experimental test rig

The hydraulic bench described in Ref. 5 was used in this work. A schematic is shown in Fig. 2. It consists of two reservoirs of identical cross section (1800 cm^2), filled with water up to a height h = 40 cm, separated by a distance L = 400 cm, and connected by two rigid pipes of polyvinyl chloride (PVC, ISO 1452). Rigid pipe 1 connects the compliant tube to reservoir 1 and rigid pipe 2 connects the compliant tube to reservoir 2. The rigid pipes have an inner diameter D = 16 mm. L_1 and L_2 are the distances between the compliant tube symmetry plane and reservoirs 1 and 2, respectively. The length ratio λ = L_2/L_1. The rigid tubes are joined by a latex compliant tube constructed by the authors and have the mechanical properties determined in previous studies. [25] The compliant tube has a length L_3 = 10 cm, an inner diameter D_C = 20 mm, and a wall thickness wt = 0.7 mm. The distance between the compliant tube symmetry plane and the pinching symmetry plane is defined as L_4. The impedance position ratio $\chi = L_4/\left(\frac{L_3}{2}\right)$. The width of the pinching region is a = 2 cm. In the present study, the geometrical parameters h, L, D, L_3, D_C, wt, and a were kept fixed. To carry out the tests under steady conditions, the two reservoirs were connected by means of a 20-mm-diameter silicone return pipe equipped with a gate valve. Water was used as the working fluid.

In this installation, the instrumentation consisted of four unidirectional ultrasonic flowmeters (Sonotec Sonoflow CO.55/239H V2.0, Germany) and a pressure meter (Keller PD-23, Switzerland). The flowmeters, arranged in pairs (F1-F2 in rigid pipe 1 and F3-F4 in rigid pipe 2) were used to measure the instantaneous flow rates Q_1 and Q_2 in rigid pipes 1 and 2, respectively. The pressure meter was placed in reservoir 2 to measure the variation of the water level in this reservoir during non-steady tests and thus the head increase. The data acquisition system was based on an Arduino Due® board that recorded the instantaneous values measured by the instruments with a time resolution of 1 ms. The pressure and flow meter uncertainties were 4% and 2% of the full scale of the instrument, respectively.

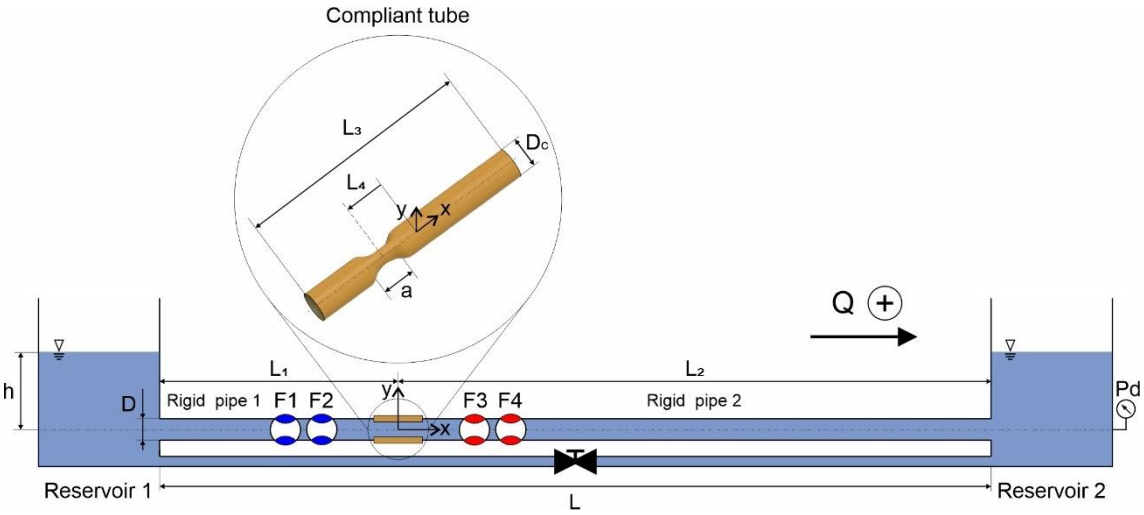

FIG. 2. A schematic diagram of the Liebau pumping test rig with an illustrative subpanel showing the compliant tube and its pinching region.

1- Soft robotic pincher

The pincher used is based on soft robotics technology, which has the advantages over other possible systems of a smaller size, biocompatibility, and increased durability of the compliant tube, as described in Ref. 5. The design was modified from previous work [Fig. 3(a)] to allow evaluation of the evolution of the deformation of the compliant tube. In addition, this new design can facilitate the future use of the Liebau pump in extracorporeal circulation devices, as it facilitates line exchange.

The soft robotic pincher consists of two identical modules that are placed opposite to each other on both sides of the compliant tube so that their implementation does not require disconnecting the compliant tube from the rigid pipes, as was the case with the previous pincher.[5,25] Each module of the soft robot is an orthohedron (43 mm × 43 mm × 25 mm) made of platinum silicone Easyplat 00-30 (Feroca, Spain), with a hollow chamber inside (25 mm × 25 mm × 4 mm). This is placed inside rigid polylactic acid (PLA) housing, allowing it to deform only toward the compliant tube [Fig. 3(b)]. The soft robot is pneumatically driven by compressed air at an operating pressure P_t.

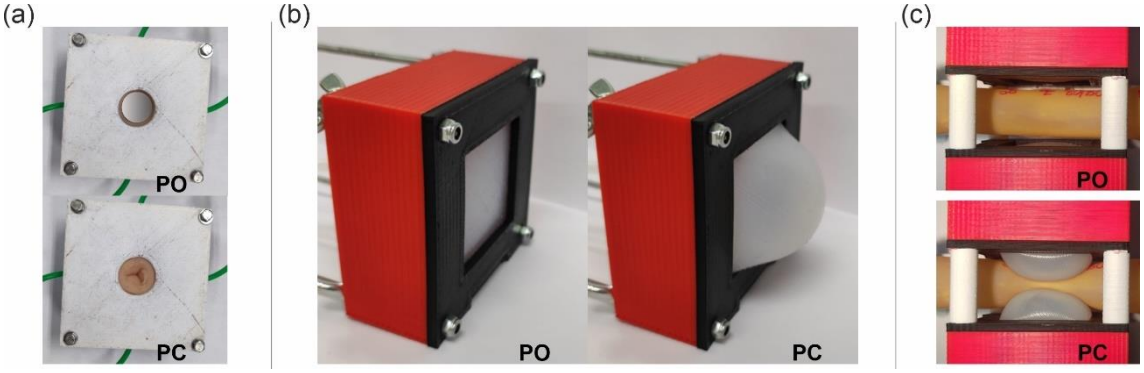

FIG. 3. (a) The soft robot used in previous works. (b) A module of the soft robot inside its rigid casing (in red), in its resting state (left), and being deformed by compressed air (right). (c) Upper: the soft robot pincher not compressing the compliant tube. Bottom: the pincher compressing the compliant tube. PO = Pincher open, PC = Pincher closed.

2- Pinching frequency control system

The operating cycle of the soft robot has two phases. In the first phase (pincher closed, PC) the compressed air enters the internal chamber of the soft robot, causing its wall to deform toward the compliant tube and compress it [Fig. 3(c)]. This drives the fluid inside the compliant tube toward its ends. In the second phase (pincher open, PO), the chamber is depressurized, and the soft robot recovers its initial shape. The percentage of the operating cycle in which the pincher is closed, compressing the compliant tube, is called the duty cycle.[16,19] Previous work[5] showed that an adequate duty cycle (γ) corresponds to a value of 33% since a lower value result in incomplete compression of the compliant tube and a higher value is inefficient because it can make refilling difficult. In this study, it is also observed that for a value of 33%, the closure is complete. Therefore, this value was set as the nominal value of the duty cycle for the tests carried out in this work.

To set the period of the operating cycle (T) or its inverse, the pinching frequency (*f*), a control system is needed. This system, based on Arduino Nano®, allows for the setting of the pinching frequency in two ways. The manual frequency mode allows the setting of a certain pinching frequency that remains constant during the test. The automatic frequency mode allows the resonant frequency (f_R), which is the optimal pinching frequency in each pump duty cycle, to be determined for each configuration. The pinching frequency has a time resolution of 1 ms and was recorded by the data acquisition system.

In most previous works carried out on the Liebau pump, the pinching frequency was set manually[16,19] and the methodology usually used to determine the resonant frequency was to perform a frequency sweep. In Ref. 25, a methodology was proposed to determine this resonant frequency from the instantaneous flow rate signal in rigid pipe 1 (which corresponds to the automatic frequency mode of the flowmeter). The resonant period corresponded to the time between two consecutive maxima of the instantaneous flow rate at the junction of rigid pipe 1 and the compliant tube. In the present work, we have improved the methodology for capturing the resonant frequency using the capacitance variation (C) of a parallel plate capacitor [Fig. 4(a)] with the dimensions shown in Fig. 4(b). The plates are placed on both sides of the compliant tube in a location near the pincher, on the rigid pipe 2 side as seen in Fig. 4(c), 4(d) and 4(e).

The capacitance change between the plates of the capacitor is caused by the deformation of the compliant tube when it is compressed. In a capacitor, if the plates have a fixed surface area and the distance between them does not vary, the capacitance is proportional to the permittivity of the dielectric between them. Thus, it is different when the compliant tube is filled with fluid (high permittivity, high capacitance), as seen in Fig. 4(e), and when it is empty (low permittivity, low capacitance), as seen in Fig. 4(d). In this way, the capacitance changes allow us to determine the time interval that exists between two refills of the compliant tube and to command the pincher to close. This time interval is the resonant period and determines the resonant pinching frequency in each operating cycle (in the automatic frequency mode by capacitance).

Capacimeters are often used to measure capacitance changes. However, this method does not suit our need for fast sampling. Therefore, a circuit with an LM555 astable oscillator was used, which generates a square wave from the capacitor charge and discharge times. The period depends on the circuit resistance and capacitance. As the resistance has a fixed value, we obtain a frequency associated with the period of the oscillator signal, which varies with the capacitance. In Fig. 4(f), we visualize the time evolution of the capacitance with respect to the capacitance value when the compliant tube is undeformed (C_{REF}). The capacitance change is produced by the amount of water that exists at each moment in the region of the compliant tube located between the plates of the condenser. Values below one imply that the tube contains less water than its capacity at rest, while values above one imply that the tube contains more water. It can be seen that the sudden closure of the soft robotic pincher leads to an instantaneous accumulation of water and consequently, a swelling at the ends of the compliant tube. Later, this accumulated water travels into both reservoirs, emptying the compliant tube. Fig. 4(f) shows the time evolution of the positive Q_1.

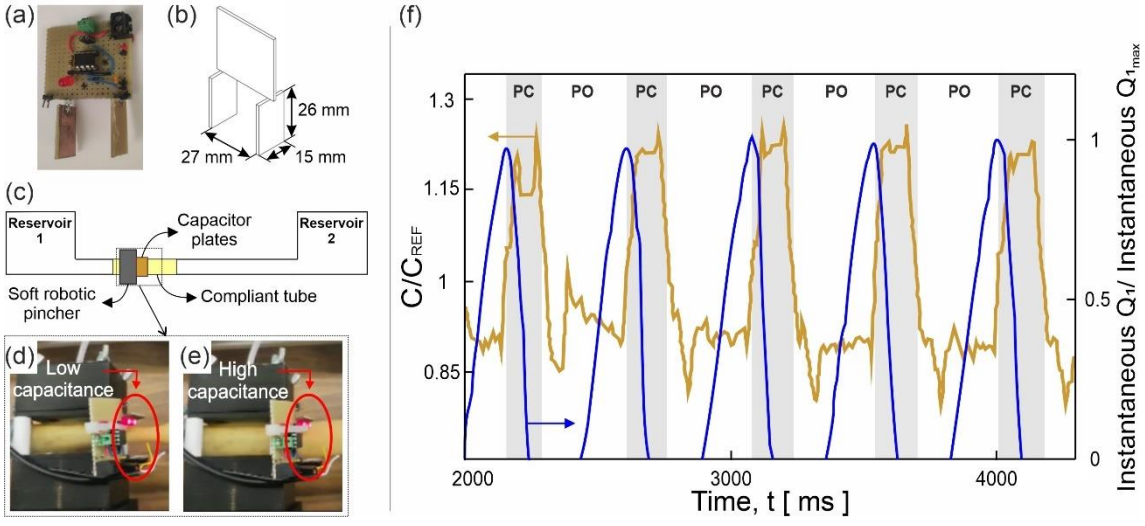

FIG. 4. (a) The parallel plate capacitor and (b) its dimensions. (c) The position of the capacitor in the test rig. The capacitor is attached to the soft robot housing to measure the dielectric capacitance for (d) low capacitance and (e) high capacitance. When the pinch region is empty, the capacitance is low, while when the pinch region is completely filled of fluid the capacitance is high. (f) The time evolution of the capacitance normalized with respect to the reference capacitance (C_{REF}, ochre) and the positive instantaneous flow rate in rigid pipe 1 (blue).

B- Operation

In this experimental study, both steady and non-steady tests were performed. In the steady tests, the two reservoirs were interconnected by means of the return pipe, and the pump operated at a single operating point close to the maximum flow rate.

In the non-steady tests, the reservoir return pipe was closed. In this way, it was possible to see the time evolution of the pump through all its operating points, from the maximum net flow rate to the maximum head. The initial condition was that the reservoirs had the same water level (h). The evolution of the net flow rate and the difference in head between the reservoirs and resonant frequency were recorded until the maximum head was reached. The maximum net flow rate obtained in the non-steady tests occurred at t = 0, when pumping started and the heads in both reservoirs were equal. These tests made it possible to obtain the characteristic curve of the pump.

Thereafter, in each series of tests, the test conditions were specified at the beginning of their respective sections. The relevant test conditions to be set were as follows: steady or non-steady test, established pumping mechanism, selected frequency mode, geometric parameters of the installation, and operating parameters (P_t and γ). First, asymmetric pumping tests were carried out to evaluate the pump performance with the new soft robotic pincher and capacitive frequency control system, and to compare them with those obtained in Ref. 5. Second, the different pumping mechanisms of the Liebau pump as a function of the operating pressure of the compressed air line P_t were studied, both separately [Figs. 1(b) and 1(c)] and together [Fig. 1(d)]. A symmetric system was also analyzed [Fig. 1(a)]. Finally, tests were carried out to analyze the possibility of replacing the reservoirs with compliant chambers to achieve a smaller and watertight configuration for future applications in medical devices.

III- RESULTS

A- Comparison with previous asymmetric pumping devices

1- Soft robotic pincher with circular closure versus planar closure

The results shown in this section compare the circular closure soft robot (CSR) used in Ref. 5 [Fig. 3(a)] with the planar closure soft robot (PSR) used in the present study [Fig. 3(b)]. All parameters shown in Table I were maintained in the tests with both pinchers. PSR was designed to compress the same length of compliant tube as CSR. In this way, it is possible to compare how the new way of compressing the compliant tube affects the performance of the pump.

The test conditions were a steady test, asymmetric pumping, and fixed geometric parameters and operating parameters [Table I]. The frequency control system was in automatic frequency mode.

Table I. The geometric and operating parameters for both soft robots.

Parameter	h	D	D_C	L_3	wt	a	L
Value	40 cm	16 mm	20 mm	10 cm	0.7 mm	2 cm	400 cm
Parameter	L_1	L_2	λ	L_4	χ	P_t	γ
Value	75 cm	325 cm	4.3	0 cm	0	1–1.4 bar	33%

Figure 5(a) shows the net pumped flow rate for different operating pressures (P_t). For both pinchers, the flow rate increases with P_t. The speed at which the soft robotic pincher deforms the compliant tube increases with pressure, and thus, so do the instantaneous flow rate and the net flow rate. Under the same operating pressure, the flow rate pumped by the new planar pincher (PSR) is 14% higher.

Figure 5(b) shows the changes in the resonant frequency with the operating pressure. An increasing trend is observed for the PSR and a slightly decreasing trend for the CSR. The resonant frequency depends on the geometrical parameters of the installation and the deformation of the compliant tube since these determine the pressure gradients and therefore the characteristics of the instantaneous flow rate waves. It is seen that over the entire operating pressure range, the CSR is able to close completely and therefore its frequency plot shows little variation with operating pressure. However, in the case of the

PSR, a higher operating pressure implies that the closure is performed in less time, therefore leading to higher frequencies.

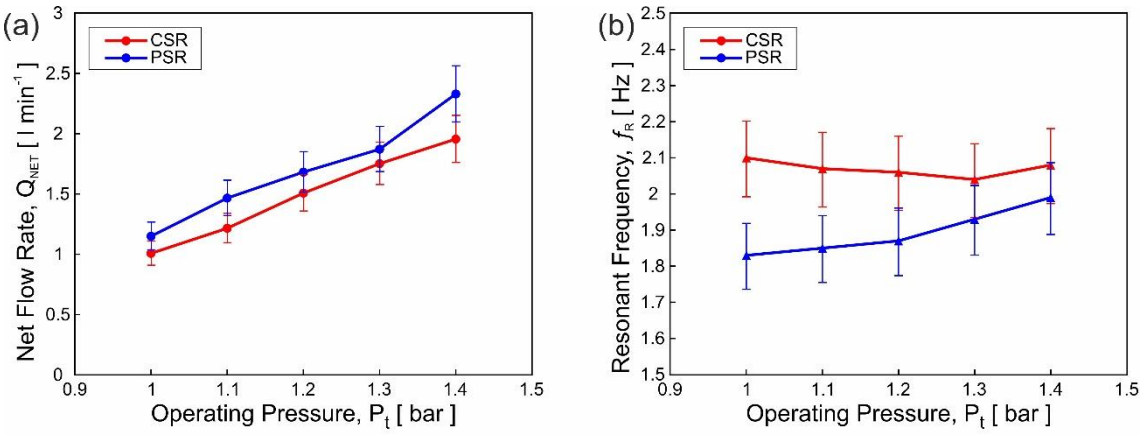

FIG. 5. Changes in the (a) net flow rate and (b) resonant frequency with the operating pressure. Each data point is calculated by averaging the net flow rate and the resonant frequency of 121 consecutive cycles. Error bars represent one standard deviation.

In manual frequency mode, a pinching frequency sweep was performed with P_t = 1.4 bar. Figure 6 shows the ratio of the net flow rate (Q_{NET}) to its maximum value (Q_{NETmax}) versus the ratio of the pinching frequency (f) to the resonant frequency (f_R) for both soft robotic pinchers. It is observed that the behavior pattern is similar to that described in other works,[19] i.e., a nonlinear and pronounced variation of the flow rate with frequency is seen, along with a reverse flow rate for frequencies far from the resonant frequency. Although the PSR has a narrower positive flow rate range of frequencies, this is not a disadvantage, since these systems work at their resonant frequency to obtain maximum performance. For the present study, it was decided to use the PSR pincher because of its higher net flow rate and ease of installation.

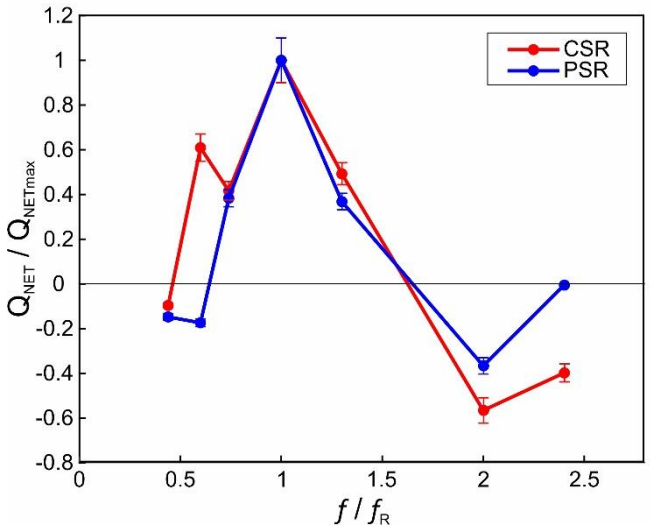

FIG. 6. The ratio of the non-dimensional net flow rate to its maximum value for a frequency sweep for both soft robotic pinchers. Each data point is calculated by averaging the net flow rate of 121 consecutive cycles. Error bars represent one standard deviation.

2- Frequency control by flowmeter and capacitance

For optimum pump performance, it is important to determine the resonant frequency (f_R). The nature of the Liebau effect is complex and many factors influence the resonant frequency. It is therefore essential to establish a methodology to determine it. For this series of tests, the test conditions were: steady tests, asymmetric pumping, the parameters indicated in Table I, and an operating pressure of P_t = 1.1 bar.

First, in manual frequency mode (MFM), a frequency sweep was performed with a higher resolution than in Fig. 6, around the resonant frequency. Figure 7 shows the non-dimensional net flow rates for frequencies close to the resonant frequency. Then, working in automatic frequency mode by capacitance (AFMC), the frequency indicated by the blue circle in Fig. 7 was determined, which coincides with the resonant frequency (the one that gave the best performance in the manual sweep). Finally, a test was performed by setting the automatic frequency mode with the flowmeter (AFMF), as was already done in Ref. 5, and the frequency indicated by the red circle was obtained (Fig. 7). It is observed that the methodology based on the capacitance change more accurately determines the resonant frequency. In addition, the considered device is more compact and therefore more implantable. Thus, it is concluded that the resonant frequency detection system is an improvement over that used in previous work. The automatic frequency mode by capacitance (AFMC) approach is adopted for the present study.

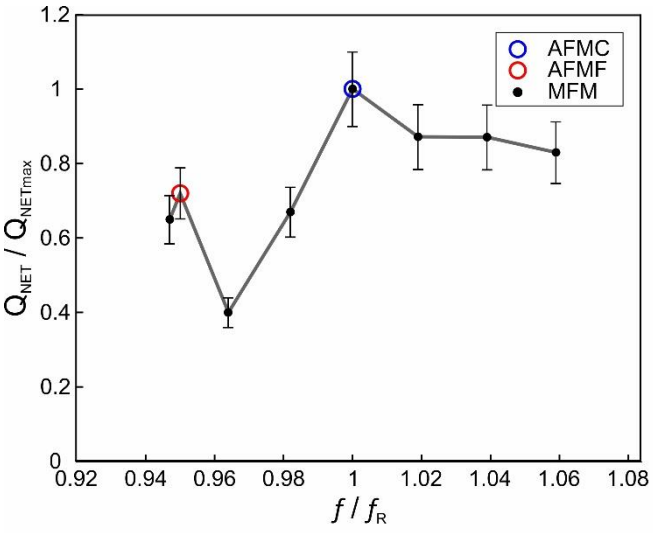

FIG. 7. The net flow rate non-dimensionalized with its maximum value as a function of the pinching frequency for values close to the resonant frequency. The blue circle shows the automatic frequency mode by capacitance. The red circle indicates the automatic frequency mode by flowmeter. Each data point is calculated by averaging the net flow rate and the resonant frequency of 121 consecutive cycles. Error bars represent one standard deviation.

B- Pumping modes and the Liebau effect

As reported in Ref. 5, Liebau effect pumping consists of two mechanisms: asymmetric pumping and so-called impedance pumping. In this section, the performance characteristics of both of these mechanisms are analyzed independently and in combination. For this purpose, five configurations are established: symmetric, impedance, asymmetric, Liebau 1, and Liebau 2. Figure 8(a) shows each of these configurations, which are characterized by the position of the pinching region in the compliant tube (impedance position ratio, χ) and the lengths of the rigid pipes (length ratio, λ). In this section, the PSR with the AFMC frequency mode and a duty cycle of γ = 33% were used.

Figures 8(b) to 8(f) show the evolution of the instantaneous flow rates in rigid pipe 1 and rigid pipe 2, Q_1 and Q_2, respectively, using the phase average calculated from data from 121 consecutive operating cycles for a steady test. The data dispersion was below 5%. Positive flow rates correspond to a flow direction from reservoir 1 to 2. The operating pressure was P_t = 1.1 bar. The magnitude of the instantaneous flow rate wave in both pipes was determined by the position of the pincher in the compliant tube and the inertia and loss terms associated with each pipe.

Figure 8(b) shows that, for the symmetrical configuration, the evolution of the instantaneous flow rate through both pipes is symmetrical. The resulting net flow rate is practically zero. To be completely zero, the pincher would have to act exactly in the plane of symmetry of the compliant tube and the circuit. This is experimentally very complicated because millimeter differences in the value of L_4 can cause the flow rate to be non-zero.[11,15,16]

If the symmetry is broken by shifting the position of the pincher with respect to the plane of symmetry of the compliant tube (χ = −0.5), maintaining the length ratio (λ = 1), we have an impedance pump. In this case, the instantaneous flow rate amplitude Q_2 is larger than Q_1 [Fig. 8(c)] and the net flow rate has a value of Q_{NET} = 1.93 l min^{-1}. In Fig. 8(c), it can be seen that the flow rate wave of rigid pipe 1 has a different dynamic than that of rigid pipe 2. The main effect that occurs is that the instantaneous flow rate Q_1 changes

to positive values very quickly due to the suction exerted by the pressure waves reflected in the compliant tube. It should be noted that the pressure waves traveling through the compliant tube bounce off at the impedance change (compliant tube-rigid pipe junction) and in this case, because the compliant tube is compressed out of the plane of symmetry, they do not cancel out when they meet.[11]

If the symmetry is broken by modifying the length ratio ($\lambda = 4.3$), but the pincher acts in the symmetry plane of the compliant tube ($\chi = 0$), we have an asymmetric pump. In this case, $Q_{NET} = 1.47$ l min^{-1}. The instantaneous flow rate amplitude Q_1 is larger than Q_2 [Fig. 8(d)], which is opposite to the effect of the impedance, where Q_2 was larger than Q_1. Rigid pipe 1 has less inertia and losses than rigid pipe 2 because it is much shorter in length. Therefore, the amplitude of the flow rate going to reservoir 1 is greater.[23]

If the symmetry is broken by shifting the pincher position and by modifying the length ratio, we have a Liebau pump. In the Liebau 1 configuration, the two previous effects [impedance ($\chi = -0.5$) and asymmetry ($\lambda = 4.3$)] are combined, and it can be seen that the maxima of the instantaneous flow rate [Fig. 8(e)] have intermediate values between the two previous effects. This suggests that both effects are combined but the superposition principle cannot be applied, since both are interrelated. The net flow rate for this configuration is $Q_{NET} = 2.90$ l min^{-1}, lower than the sum of the separate effects. When $\chi = 0.5$ and $\lambda = 4.3$, we have the Liebau 2 configuration, in which the two mechanisms pump in opposite directions, resulting in $Q_{NET} = 0.38$ l min^{-1}. The instantaneous flow rate amplitude Q_1 is larger than Q_2 [Fig. 8(f)].

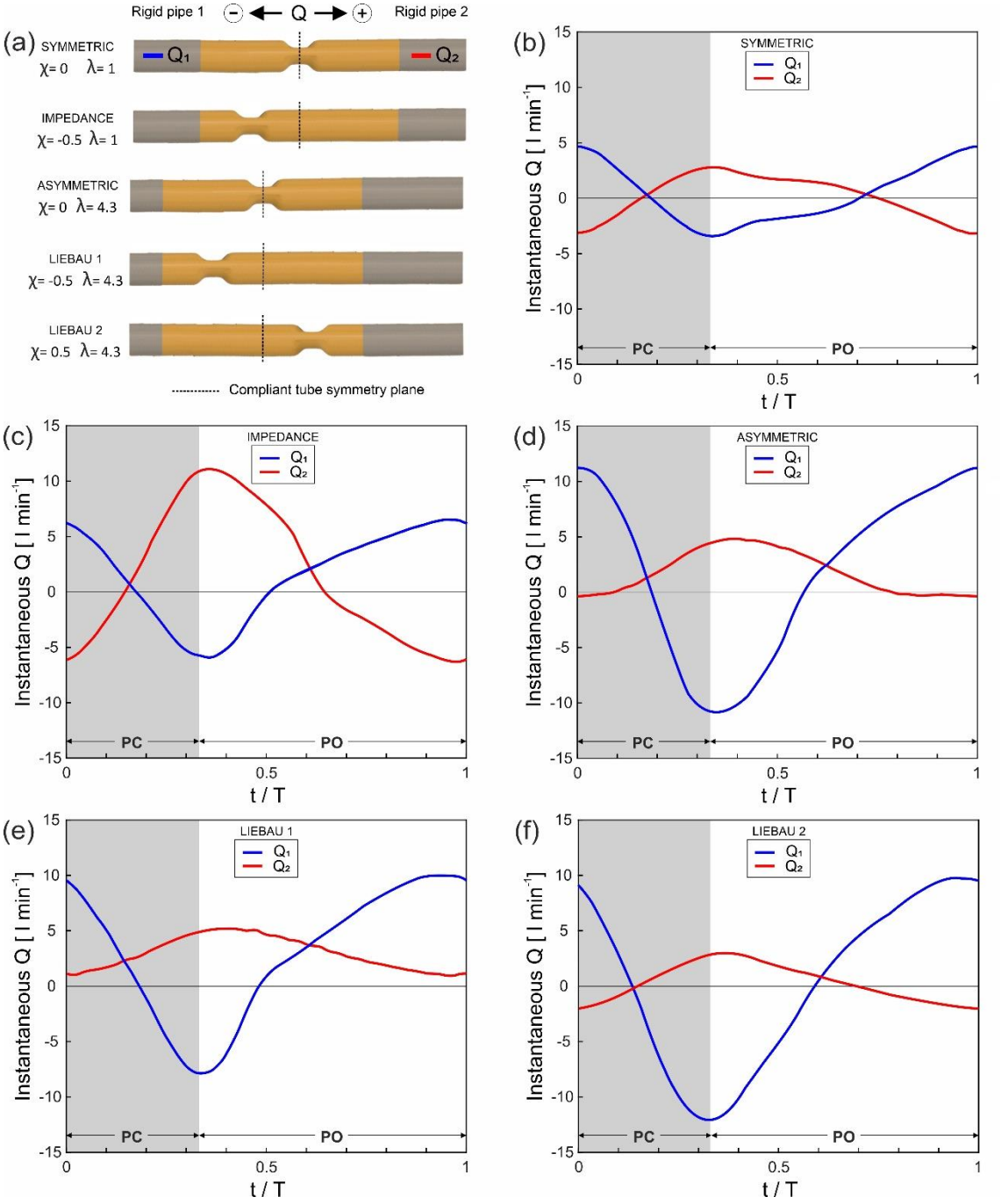

FIG. 8. (a) The compliant tube with its associated impedance position ratio and length ratio for each pumping mode. (b) The evolution of the instantaneous flow rates in the rigid pipes during a period (T) of the operating cycle. Q_1: The phase-averaged instantaneous flow rate in rigid pipe 1, Q_2: The phase-averaged instantaneous flow rate in rigid pipe 2. The pincher is closed for 33% of T (PC). The phase averages are calculated from data from 121 consecutive operating cycles. T = 602 ms, (c) T = 602 ms, (d) T = 541 ms, (e) T = 474 ms, (f) T = 549 ms.

Figure 9(a) shows the changes in the net flow rates with the operating pressure for the different pumping configurations, with the flow rates increasing with P_t. Figure 9(b) shows

the resonant frequency for each of the configurations. The trend is that it increases slightly with the operating pressure. Over the whole range of pressures, the highest resonant frequency is for the Liebau 1 configuration, there is a lower resonant frequency for the asymmetric pumping configuration and for Liebau 2, and finally, the lowest frequency is seen for the impedance and symmetry configurations.

As explained in Refs. 5 and 25, the resonance frequency of the asymmetric configuration is given by the evolution of the flow rate in the short pipe. The Liebau 2 configuration shares this short pipe, which is where the compliant tube is filled, but with the addition that the impedance opposes the asymmetry effect without canceling it out, and therefore, its resonance frequency is slightly slower than that obtained for pure asymmetry. In the symmetry and impedance configurations, both pipes are equally long. As the suction pipe is longer than in the asymmetry case, it has more inertia to overcome, and hence the resonant frequency of the circuit is lower. Finally, Liebau 1 shares all the above features, with the suction pipe the same as in the asymmetry case, but with the addition of the suction effect provided by the impedance, which results in a much higher resonance frequency than in the other two cases. In view of the performance findings, the tests were continued by adopting the Liebau 1 pumping configuration.

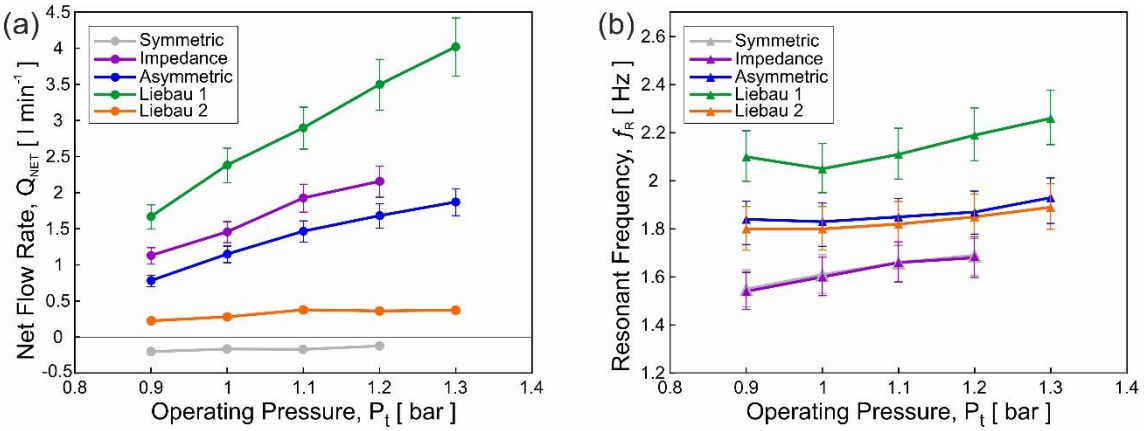

FIG. 9. Changes in the (a) net flow rate and (b) resonant frequency with the operating pressure for the different pumping configurations. Each data point is calculated by averaging the net flow rate and the resonant frequency of 121 consecutive cycles. Error bars represent one standard deviation.

C- Compliant chambers

1. - Justification and operation

The possible clinical applications of the Liebau pump, e.g., in extracorporeal blood circulation, require a compact configuration that can be easily incorporated into a circuit and with a pulsatile flow rate. For this purpose, it is envisaged that the reservoirs could

be replaced with easily integrable compliant chambers (CCs). CCs can dampen the instantaneous flow rate fluctuations (Fig. 8) and could be designed according to pulsatility needs, either reducing the fluctuations or eliminating them completely depending on the requirements. Another purpose of CCs is to avoid the reverse flow that occurs at certain periods during the operating cycle.

In the Liebau 1 configuration, which showed the highest performance, there was no reverse flow or high instantaneous flow fluctuations in rigid pipe 2 [Fig. 8(d)] so it was decided to use only one CC in rigid pipe 1 to minimize the reverse flow and dampen the instantaneous flow fluctuations in this pipe. The resulting Liebau pump consisted of a suction pipe, a compliant chamber, a rigid intermediate pipe, a compliant tube with a soft robot pincher, and a rigid impulsion pipe.

It is important for future applications that the working fluid is not in contact with air, so the compliant chamber is designed as a closed, fluid-filled system. The compliant chamber works as an energy accumulator that dampens the upstream flow and pressure variations. As it is a closed chamber, the overpressures are absorbed by the deformation of the elastic walls of the CC.

2. – Experimental test rig with compliant chamber

To analyze the influence of the CC on the performance of the Liebau pump, the installation described in Section 2.1 was modified and a compliant chamber (CC) was installed, as seen in Fig. 10. The CC was composed of a latex tube (wt_{CC} = 0.3 mm, D_{CC} = 20 mm, and L_{CC} = 30 cm), constructed using the same methodology as for the compliant tube, thus its compliant can be addressed in Ref. 25 in terms of the wt. The compliant chamber was filled with water and was placed transversely. The CC divided rigid pipe 1 into two sections: the intermediate pipe (between the CC and the compliant tube) and the suction pipe. The compliant chamber was located at a distance L_5 from the symmetry plane of the compliant tube and at a distance L_6 from reservoir 1 ($L_5 + L_6 = L_1$). Rigid pipe 2 was renamed the impulsion pipe (discharge pipe). The length ratio $\lambda_M = L_2/L_5$. The flowmeter pairs F1-F2, F3-F4, and the additional F5-F6 measured the instantaneous flow rates in the suction pipe, intermediate pipe, and impulsion pipe, respectively, as seen in Fig. 10.

The influence of varying L_{CC}, wt_{CC}, and λ_M on the damping of the instantaneous flow rate and the reverse flow to pipe 1 was analyzed for a Liebau pump. The test conditions in this experimental series were: the Liebau pumping configuration, automatic frequency mode by capacitance (AFMC), the duty cycle at its nominal value of 33%, and steady and non-steady tests.

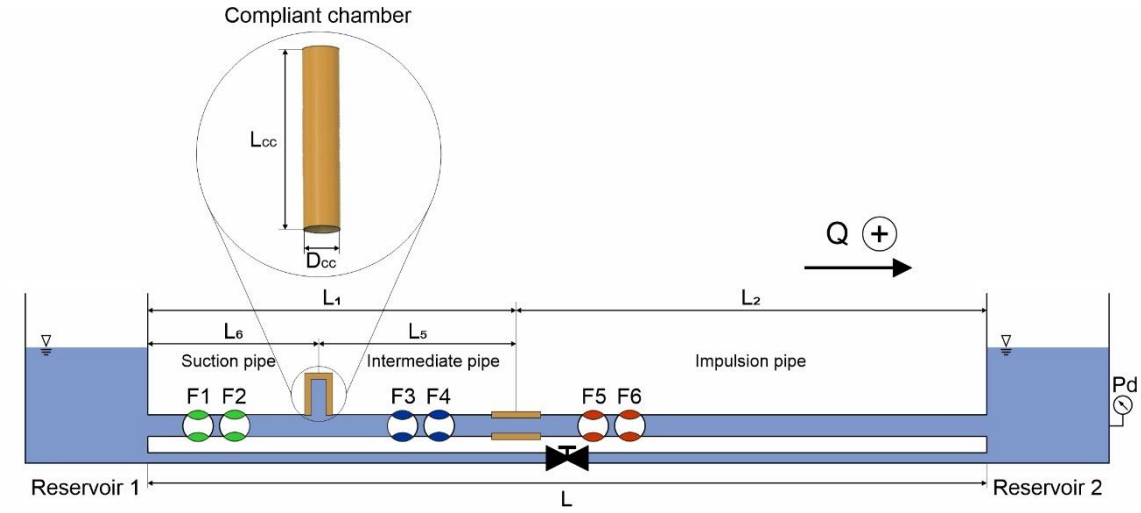

FIG. 10. A schematic diagram of the Liebau pumping test rig with an illustrative subpanel showing the compliant chamber.

3.- Influence of the compliant chamber length

In this series of steady tests, the operating pressure of P_t = 1.1 bar and the geometrical length parameters shown in Table II were established.

Table II. Geometrical length parameters in the test rig with the compliant chamber.

Parameter	L	L_1	L_2	L_5	L_6	λ	$λ_M$
Value	400 cm	119 cm	281 cm	65 cm	54 cm	2.4	4.3

Figure 11 shows the time evolution of the instantaneous flow rate in the installation shown in Fig. 10. It is observed that when there is no CC, the instantaneous flow rate in rigid pipe 2 [the red curve in Fig. 11(a)] has a pulsating flow rate with practically no reverse flow. However, the instantaneous flow rate in rigid pipe 1 (blue curve) has very strong fluctuations and a reverse flow rate range, which are not desirable characteristics.

Figures 11(b), 11(c), and 11(d) show the influence of the length of the compliant chamber L_{CC} on the time evolution of the instantaneous flow rates. In the intermediate pipe section, the flow rate characteristics in rigid pipe 1 when there is no compliant chamber (blue curve) are maintained. For all L_{CC}, the instantaneous flow rate in the impulsion pipe (red curve) has no reverse flow. In the suction pipe, the reverse flow is much lower, and the flow rate fluctuations have been damped (green curve). Therefore, the main objective of the CCs is achieved if lengths over 10 cm are used. With this configuration, the implementation of the Liebau pump in a circuit would imply a pulsating flow in the impulsion and suction pipes with no reverse flow.

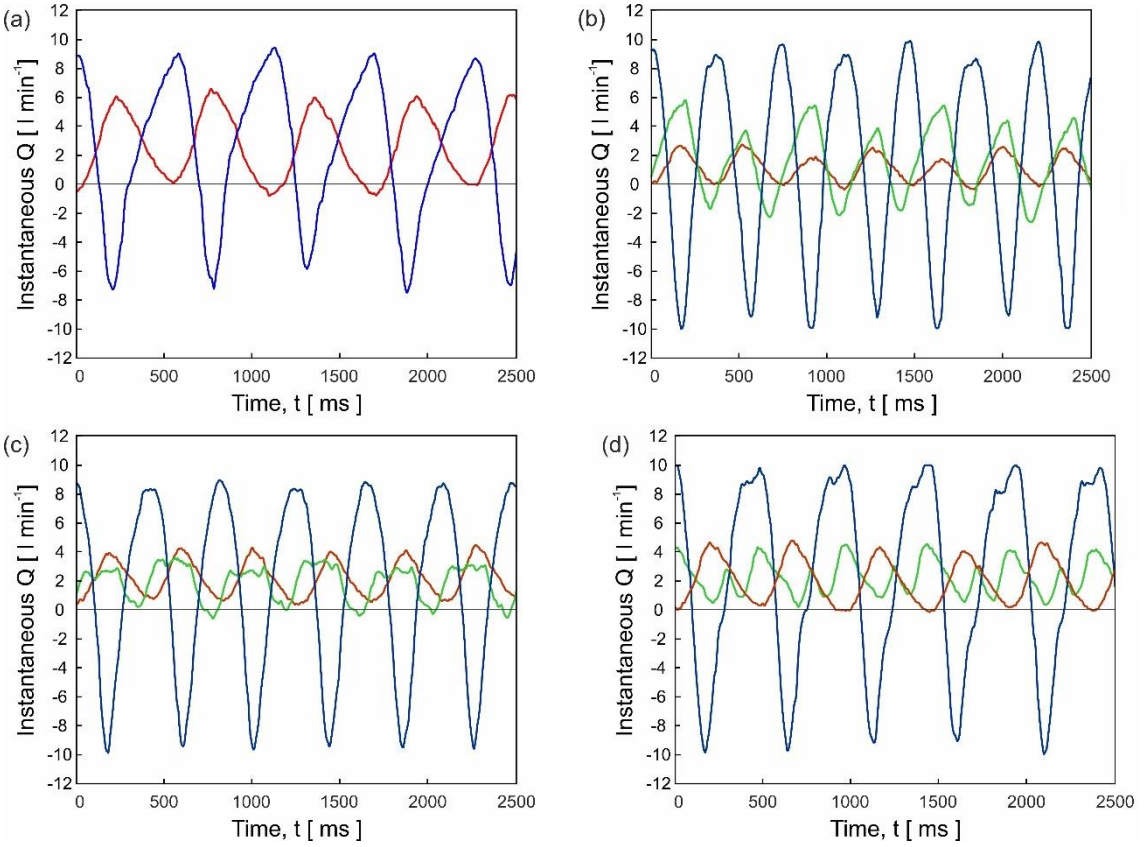

FIG. 11. (a) The evolution of the instantaneous flow rates in rigid pipe 1 (blue) and rigid pipe 2 (red) without the CC. The evolution of the instantaneous flow rates in the suction pipe (green), the intermediate pipe (blue), and the impulsion pipe (red) with the CC, for (b) L_{CC} = 10 cm, (c) L_{CC} = 20 cm, and (d) L_{CC} = 30 cm.

Figure 11 shows that as the length of the compliant chamber (L_{CC}) increases, the flow rate in the suction pipe (green curve) is less pulsating and there is no reverse flow. The presence of the CC produces a lag between the flow rate in the suction pipe and the flow rate in the intermediate pipe. When the pincher closes, both pipes (intermediate and suction) fill the compliant tube. When the pincher closes, only the flow in the intermediate pipe tends to change direction, resulting in the filling of the CC on both sides (intermediate and suction). When the pincher opens, the CC is emptied in both directions, both toward the compliant tube and toward the reservoir. Due to this, the waves are out of phase, making the CC independent of the flow rate evolution in both pipelines.

The best configuration in these terms is that with the CC with the longest length because a larger volume for the compliant chamber allows better damping of the overpressure. In addition, by eliminating the reverse flow, this configuration provides the best performance in terms of the flow rate considered (Q_{NET} = 2.22 l min^{-1}). Figure 11 also shows that the

operating cycle period increases with L_{CC}. Based on these results, L_{CC} = 30 cm was adopted for the remainder of the tests.

4. -Influence of the compliant chamber wall thickness

This section analyzes the influence of the CC wall thickness (wt_{CC}) on the damping effect and pump performance. The stiffness of the compliant chamber was increased by setting wt_{CC} = 0.8 mm and the configuration and test conditions of the previous section were maintained. The instantaneous flow rates were measured in the different pipes, as seen in Fig. 12.

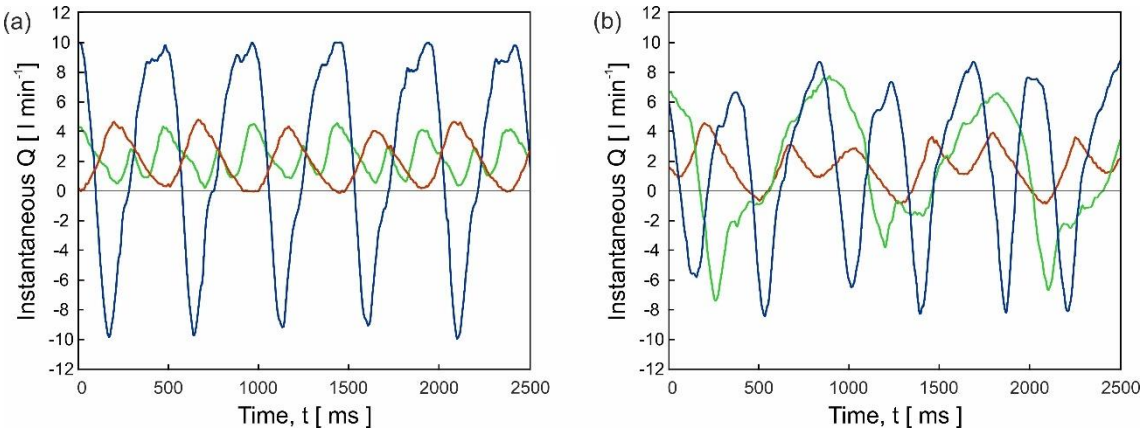

FIG. 12. The evolution of the instantaneous flow rates in the suction pipe (green curve), the intermediate pipe (blue curve), and the impulsion pipe (red curve) for different wall thicknesses (wt_{CC}): (a) wt_{CC} = 0.3 mm and (b) wt_{CC} = 0.8 mm.

As the wall thickness increases, the damping effect is lost because the wall loses elasticity. In this case, there is no phase shift between the flow rate waves and the instantaneous flow rate is very chaotic. With this configuration, the net flow rate is reduced by 24 %. As a result, wt_{CC} = 0.3 mm is adopted for the remainder of the tests.

5. - Influence of the length ratio

In this series of steady tests, the influence of the length ratio ($\lambda_M = L_2/L_5$) on the damping of the instantaneous flow rate flowing through the suction pipe is analyzed, since λ_M determines the dimensions of the Liebau pump prototype. In these tests, the installation lengths were L_1 = 157 cm and L_2 = 243 cm, and L_5 was varied to obtain λ_M = 8.4, λ_M = 3.7, and λ_M = 2.4. The rest of the test conditions were maintained as in the previous tests with a compliant chamber.

Figure 13(a) shows that as the operating pressure increases, the net flow rate increases for all length ratios. It is observed that for a fixed operating pressure (e. g. P_t = 1.2 bar),

the net flow rate shows a maximum for λ_M close to 4. This behavior is similar to that seen in Ref. 5.

If we analyze the time evolution of the instantaneous flow rate in the suction pipe for similar net flow rates, of the order 2.3 l min^{-1}, we can see how the damping improves with increasing λ_M, that is, with decreasing L_5 [Figs. 13(b), 13(c), and 13(d)].

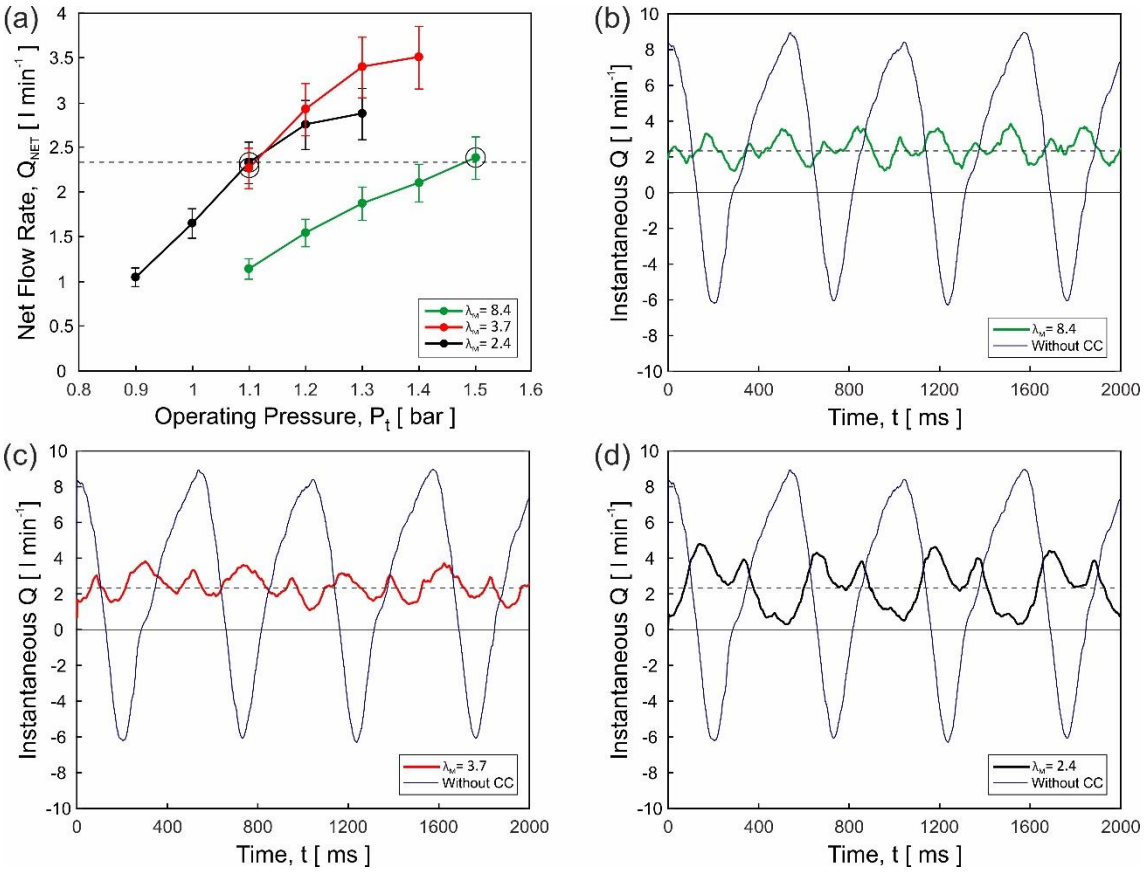

FIG. 13. (a) The net flow rate at the operating pressure for different prototype length ratios. Each data point is calculated by averaging the net flow rate of 121 consecutive cycles. Error bars represent one standard deviation. (b) For Q_{NET} = 2.3 l min^{-1} (dashed line), the evolution of the instantaneous flow rates in the suction pipe for different prototype length ratios (λ_M) compared with the instantaneous flow rate without a compliant chamber in that pipe for λ_M = 8.4, (c) λ_M = 3.7, and (d) λ_M = 2.4.

D. -Adaptability for biomedical purposes

As already shown by several authors,[1,29] Liebau pumps have suitable characteristics for use in biomedical applications, such as a compact and simple design, the absence of valves that can damage biofluids, and a pulsating flow. The lack of pulsatility in a pulmonary arterial flow rate has been shown to cause pulmonary vascular reduced nitric oxide synthetase and endothelial dysfunction, and ultimately, elevated pulmonary vascular resistance.[30]

A non-steady test of the Liebau pump prototype described in the previous section with the parameters indicated in Table III was carried out to determine its characteristic curve.

Table III. The geometric and operating parameters of the Liebau pump developed in this work.

Parameter	L	L_1	L_2	λ	L_4	L_5	L_6	λ_M	Pt
Value	400 cm	157 cm	243 cm	1.5	−2.5 cm	29 cm	128 cm	8.4	1.4 bar

Figure 14 shows the characteristic curve of the Liebau pump prototype alongside reference ranges for the requirements of pediatric treatment with pediatric extracorporeal ventricle assist devices (VAD). A body mass of up to 20 kg and an actuation range between 2 and 16 mmHg were considered for these ranges.[31] It is clear that the performance of the prototype Liebau pump is within the range of pediatric VAD requirements.

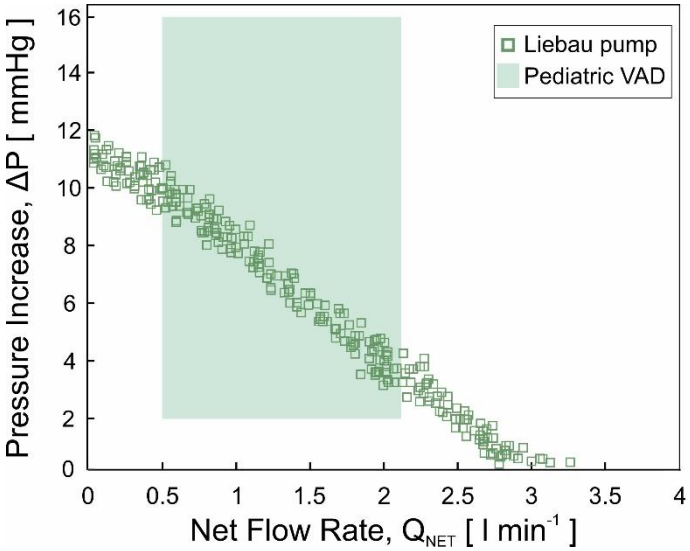

FIG. 14. Pediatric VAD application ranges overlaid on the Liebau pump characteristic curve.

IV- CONCLUSIONS

In this paper, we have compared the performance of a new soft robot and a new resonant frequency detection method with those used in previous works. The improvements in the new planar soft robot and capacitance resonant frequency detection method have been demonstrated in terms of asymmetric pumping performance and possible

implementations in biomedical applications. With these improvements, the impedance and asymmetric pumping modes, individually and jointly, have been experimentally analyzed. A mixed pumping mechanism was chosen due to its better performance. Combining these improvements, a prototype Liebau pump was developed that includes a compliant chamber to dampen flow fluctuations and reverse flow. A configuration was found for the Liebau pump prototype that preserves some pulsatility in the flow but without reverse flow, which is desirable for biofluid pumping. Finally, the results obtained from the Liebau pump module developed in this work were compared with the requirements of extracorporeal circulation devices for infants. Future work is intended to study the influence of fluid viscosity on the pump performance, the reduction in its size, and the numerical modeling of the pump.

ACKNOWLEDGMENTS

The authors would like to thank the Junta de Castilla y León for funding this work as part of the program “Subvenciones del programa de apoyo a proyectos de investigación financiados por fondos FEDER,” project number VA182P20.

AUTHORS DECLARATIONS

Conflict of interest

The authors declare that they have no conflicts to disclose.

Author contributions

J. Anatol: Conceptualization, Methodology, Investigation, Data Curation, Writing – Original Draft. **M. García-Díaz:** Conceptualization, Formal analysis, Investigation, Resources, Writing – Original Draft. **C. Barrios-Collado:** Methodology, Validation, Investigation, Data Curation, Writing – Original Draft. **J. A. Moneo-Fernández:** Software, Validation, Resources. **M. Rubio** Formal analysis, Investigation, Writing – Review & Editing. **F. Castro-Ruiz:** Conceptualization, Methodology, Investigation, Writing – Review & Editing, Visualization, Project administration. **J. Sierra-Pallares:** Formal analysis, Investigation, Writing – Review & Editing, Supervision, Funding acquisition.

DATA AVAILABILITY

The data that support the findings of this study are available from the corresponding author upon reasonable request.

Nomenclature

a	Width of the pinching region
AFMC	Automatic frequency mode by capacitance
AFMF	Automatic frequency mode by flowmeter
C	Capacitance
CC	Compliant chamber
CSR	Soft robotic pincher with circular closure
C_{REF}	Capacitance of the compliant tube at rest
D	Inner diameter of rigid pipes
D_C	Inner diameter of the compliant tube
D_{CC}	Inner diameter of the compliant chamber
f	Frequency
f_R	Resonant frequency

F1	Flowmeter in position 1
F2	Flowmeter in position 2
F3	Flowmeter in position 3
F4	Flowmeter in position 4
F5	Flowmeter in position 5
F6	Flowmeter in position 6
h	Height of water in reservoirs
L	Length between reservoirs
L_{CC}	Length of the compliant chamber
L_1	Length between reservoir 1 and the compliant tube symmetry plane
L_2	Length between reservoir 2 and the compliant tube symmetry plane
L_3	Length of the compliant tube
L_4	Length between the compliant tube and pinching region symmetry planes
L_5	Length between the compliant chamber and the compliant tube symmetry plane
L_6	Length between the compliant chamber and reservoir 1
MFM	Manual frequency mode
P	Pressure
Pd	Pressure meter in reservoir 2
PC	Pincher closed
PO	Pincher open
PSR	Soft robotic pincher with planar closure
P_t	Operating pressure
Q	Flow rate
Q_1	Flow rate in rigid pipe 1
Q_2	Flow rate in rigid pipe 2

Q_{NET}	Net flow rate
Q_{NETmax}	Maximum net flow rate
t	Time
T	Operating cycle period
wt	Wall thickness of the compliant tube
wt_{CC}	Wall thickness of the compliant chamber

Greek Symbols

γ	Duty cycle
λ	Length ratio, L_2/L_1
λ_M	Length ratio, L_2/L_5
χ	Impedance position ratio, $L_4/\left(\frac{L_3}{2}\right)$

REFERENCES

[1]N. Sarvazyan, “Building valveless impedance pumps from biological components: Progress and challenges,” Front. Physiol. 12, 770906 (2021) [DOI: 10.3389/fphys.2021.770906] [Pubmed:35173623].

[2]T. Kenner, “Biological asymmetry and cardiovascular blood transport,” Cardiovasc. Eng. 4(2), 209-218 (2004) [DOI: 10.1023/B:CARE.0000031550.14659.06].

[3]N. M. Pahlevan and M. Gharib, “In-vitro investigation of a potential wave pumping effect in human aorta,” J. Biomech. 46(13), 2122-2129 (2013) [DOI: 10.1016/j.jbiomech.2013.07.006] [Pubmed:23915578].

[4]C. Y. Wen and H. T. Chang, “Design and characterization of valveless impedance pumps,” J. Mech. 25(4), 345-354 (2009) [DOI: 10.1017/S1727719100002835].

[5]J. Anatol, M. García-Díaz, C. Barrios-Collado, J. A. Moneo-Fernández, F. Castro-Ruiz, and J. Sierra-Pallares, “Experimental characterization of an asymmetric valveless pump based on soft robotics technology,” Phys. Fluids 35(6) (2023) [DOI: 10.1063/5.0150978].

[6]S. Timmermann and J. T. Ottesen, “Novel characteristics of valveless pumping,” Phys. Fluids 21(5) (2009) [DOI: 10.1063/1.3114603].

[7]A. I. Hickerson and M. Gharib, “On the resonance of a pliant tube as a mechanism for valveless pumping,” J. Fluid Mech. 555, 141 (2006) [DOI: 10.1017/S0022112006009220].

[8]D. Auerbach, W. Moehring, and M. Moser, “An analytic approach to the Liebau problem of valveless pumping,” Cardiovasc. Eng. 4, 201 (2004).

[9]A. Aghilinejad, B. Rogers, H. Geng, and N. M. Pahlevan, “On the longitudinal wave pumping in fluid-filled compliant tubes,” Phys. Fluids 35(9) (2023) [DOI: 10.1063/5.0165150].

[10]C. F. Babbs, “Behavior of a viscoelastic valveless pump: A simple theory with experimental validation,” Biomed. Eng. 9, 42 (2010) [DOI: 10.1186/1475-925X-9-42] [Pubmed:20807440].

[11]I. Avrahami and M. Gharib, “Computational studies of resonance wave pumping in compliant tubes,” J. Fluid Mech. 608, 139-160 (2008) [DOI: 10.1017/S0022112008002012].

[12]C. G. Manopoulos, D. S. Mathioulakis, and S. G. Tsangaris, “One-dimensional model of valveless pumping in a closed loop and a numerical solution,” Phys. Fluids 18(1) (2006) [DOI: 10.1063/1.2165780].

[13]J. T. Ottesen, “Valveless pumping in a fluid-filled closed elastic tube-system: one-dimensional theory with experimental validation,” J. Math. Biol. 46(4), 309-332 (2003) [DOI: 10.1007/s00285-002-0179-1] [Pubmed:12673509].

[14]E. Jung and C. S. Peskin, “Two-dimensional simulations of valveless pumping using the immersed boundary method,” S.I.A.M. J. Sci. Comput. 23(1), 19-45 (2001) [DOI: 10.1137/S1064827500366094].

[15]A. Sharifi, A. Gendernalik, D. Garrity and D. Bark, “Valveless pumping behavior of the simulated embryonic heart tube as a function of contractile patterns and myocardial stiffness,” Biomech. Model. Mechanobiol. 20, 2001-2012 (2021) [DOI: 10.1007/s10237-021-01489-7]

[16]C. Manopoulos, S. Tsangaris, and D. Mathioulakis, “Net flow generation in closed-loop valveless pumping.,” Proc. Inst. Mech. Eng. C 234, 2126 (2020).

[17]N. G. Garafolo, B. C. Rich, and M. J. Cymbal, “An Experimental Investigation of Closed-Loop Impedance Pumping in a Compliant, Elastic Tube Millistructure by Variation of Perturbation Location,” JMDV. 5, 1 (2018).

[18]T. T. Bringley, S. Childress, N. Vandenberghe, and J. Zhang, “An experimental investigation and a simple model of a valveless pump,” Phys. Fluids 20(3), 33602 (2008) [DOI: 10.1063/1.2890790].

[19]A. I. Hickerson, D. Rinderknecht, and M. Gharib, “Experimental study of the behavior of a valveless impedance pump,” Exp. Fluids 38(4), 534-540 (2005) [DOI: 10.1007/s00348-005-0946-z].

[20]M. Pilou, Ch. Manopoulos, D. Mathioulakis, and S. Tsangaris. in *Proceedings of the 3rd IASME/WSEAS int. conf. on fluid dynamics & aerodynamics*, Corfu, Greece, *(20-22 August, 2005)*.

[21]S. J. Shin and H. J. Sung, “Three-dimensional simulation of a valveless pump,” Int. J. Heat Fluid Flow 31(5), 942-951 (2010) [DOI: 10.1016/j.ijheatfluidflow.2010.05.001].

[22]S. Takagi and K. Takahashi, “Study of a piston pump without valves: 2nd report, pumping effect and resonance in a pipe-capacity-system with a t-junction,” Bull. J.S.M.E. 28(239), 831-836 (1985) [DOI: 10.1299/jsme1958.28.831].

[23]S. Takagi and T. Saijo, “Study of a piston pump without valves: 1st report, on a pipe-capacity-system with a t-junction,” Bull. J.S.M.E. 26(218), 1366-1372 (1983) [DOI: 10.1299/jsme1958.26.1366].

[24]G. Propst, “Pumping effects in models of periodically forced flow configurations,” Phys. D Nonlinear Phenom. 217(2), 193-201 (2006) [DOI: 10.1016/j.physd.2006.04.007].

[25]J. Anatol, M. García-Díaz, C. Barrios-Collado, J. A. Moneo-Fernández, M. Horvath, T. Parra, F. Castro-Ruiz, E. T. Roche, and J. Sierra-Pallares, “Experimental study of an asymmetric valveless pump to elucidate insights into strategies for pediatric extravascular flow augmentation,” Sci. Rep. 12(1), 22165 (2022) [DOI: 10.1038/s41598-022-26524-0] [Pubmed:36550224].

[26]J. M. Floryan, S. Panday, and Kh. Md. Faisal, “On the peristaltic pumping,” Phys. Fluids 33, 033609 (2021) [DOI: 10.1063/5.0042883]

[27]Y. Aboelkassem, “Pumping flow model in a microchannel with propagative rhythmic membrane contraction,” Phys. Fluids 31, 051902 (2019) [DOI: 10.1063/1.5092295]

[28]E.-O. Jung and D.-W. Kim, “Valveless pumping in open tank system using energy conserving compartment model,” Bull. Korean Math. Soc. 49(5), 961-987 (2012) [DOI: 10.4134/BKMS.2012.49.5.961].

[29]L. Loumes, I. Avrahami, and M. Gharib, “Resonant pumping in a multilayer impedance pump,” Phys. Fluids 20, 1 (2008).

[30]Y. Zongtao, W. Huishan, W. Zengwei, Z. Hongyu, F. Minhua, L. Xinmin, Z. Nanbin, and H. Hongguang, “Experimental study of nonpulsatile flow perfusion and structural remodeling of pulmonary microcirculation vessels,” Thorac. Cardiovasc. Surg. 58(8), 468-472 (2010) [DOI: 10.1055/s-0030-1250124] [Pubmed:21110269].

[31]E. Buratto, X. T. Ye, G. King, W. Y. Shi, R. G. Weintraub, Y. d’Udekem, C. P. Brizard, and I. E. Konstantinov, “Long-term outcomes of single-ventricle palliation for unbalanced atrioventricular septal defects: Fontan survivors do better than previously thought,” J. Thorac. Cardiovasc. Surg. 153(2), 430-438 (2017) [DOI: 10.1016/j.jtcvs.2016.09.051] [Pubmed:28029339].